Pergamon

Int. J. Heat Mass Transfer. Vol. 38, No. 10, pp. 1787–1798, 1995

0017-9310/95 $9.50+0.00

0017-9310(94)00301-7

Multiple solutions for double-diffusive convection in a vertical porous enclosure

M. MAMOU, P. VASSEUR† and E. BILGEN

Ecole Polytechnique, University of Montreal, C.P 6079 Succ "Down-Town", Montreal, Quebec, Canada H3C 3A7

(*Received* 23 *July* 1994 *and in final form* 27 *September* 1994)

Abstract—A numerical study is made of double-diffusive natural convection in a rectangular fluid-saturated vertical porous enclosure. The flows are driven by conditions of uniform heat and mass fluxes imposed along the two vertical side walls of the cavity where the two buoyancy effects can either augment or counteract each other. An extensive series of numerical simulations is conducted in the range $1 \leqslant R_T \leqslant 165$, $1 \leqslant Le \leqslant 10^3$, $-20 \leqslant N \leqslant 20$ and $A = 1$, where R_T, Le, N and A are the Darcy-modified Rayleigh number, Lewis number, buoyancy ratio and aspect ratio of the enclosure, respectively. For aiding flows ($N > 0$) the behaviour of the resulting double-diffusive convection is in qualitative agreement with the available numerical results. For opposing flows ($N < 0$) the existence of multiple steady states is demonstrated. It is determined that, for a given value of N, both Lewis and Rayleigh numbers have an influence on the domain of existence of these multiple steady states. Comprehensive Nusselt and Sherwood number data are presented as functions of the governing parameters mentioned above. The effects of the buoyancy ratio are found to be rather significant on the flow pattern and heat and mass transfer, especially for the opposing flows.

INTRODUCTION

Recent interest in the study of flows with two sources of buoyancy through porous media has been mainly motivated by its importance in many natural and industrial problems. Prominent among these are the migration of moisture through air contained in fibrous insulation, grain storage, food processing and storage and contaminant transport in ground water. Double-diffusive flows through porous media are also of interest in geophysical systems, electrochemistry and metallurgy.

Early studies on double-diffusion in porous media primarily focused on the problem of convective instability in a horizontal layer. To this end Nield [1], Taunton *et al.* [2] and Rubin [3] relied on linear stability analysis to investigate the onset of thermohaline convection in a horizontal porous layer using the Darcy flow model. Poulikakos [4] studied the same problem on the basis of the Brinkman-extended Darcy model for sparsely packed porous bed. The effect of anisotropic thermo-convective currents on thermo-diffusive equilibrium in a horizontal porous layer was investigated by Malashetty [5] using linear stability analysis. Trevisan and Bejan [6] studied heat and mass transfer affected by high Rayleigh number concerning Bénard convection in a two-dimensional saturated porous layer heated from below where the buoyancy effect was due entirely to temperature gradients. Thermohaline convection in a porous medium heated and salted from below was investigated by Rosenberg and Spera [7] for a variety of boundary and initial conditions on the salinity field. Chen and Chen [8] used the Forchheimer–Brinkman extended Darcy model to account for viscous and inertia effects on double-diffusive fingering in a porous layer.

Relative to the research activity on natural convection in vertical porous enclosures driven by a single buoyancy effect, the work on convection driven by two buoyancy effects is quite limited. Bejan and his co-workers [9–11] considered natural convection heat and mass transfer in a rectangular cavity subjected to various boundary conditions. Using both analytical and numerical techniques natural convection within a porous layer subjected to heat and mass fluxes in the horizontal direction was studied for a wide range of input parameter values. A numerical study was conducted by Lin [12] to analyze the transient natural convection heat and mass transfer in a square enclosure. Influences of the governing parameters on the unsteady variations of Nusselt and Sherwood numbers were examined and discussed in detail. Mehta and Nandakumar [13] investigated the effect of non-homogeneity of the porous medium on natural convection heat and mass transfer in a saturated porous enclosure subjected to uniform fluxes of heat and mass. The resulting Nusselt and Sherwood numbers are found to be quite different from that of the homogeneous medium. Recently, Alavyoon and his co workers investigated free convection in vertical porous enclosures due to both cooperative [14] and opposing [15, 16] fluxes of heat and solute at the boundaries.

† Author to whom correspondence should be addressed.

NOMENCLATURE

A	aspect ratio, H'/L'
D	mass diffusivity
g	gravitational acceleration
H'	height of the enclosure
j'	constant mass flux
K	permeability of the porous medium
k	thermal conductivity of fluid-saturated porous medium
L'	thickness of the enclosure
Le	Lewis number, α/D
N	buoyancy ratio, $\beta_S \Delta S'/\beta_T \Delta T'$
Nu	Nusselt number, equation (11)
q'	constant heat flux
R_T	thermal Darcy–Rayleigh number, $g\beta K q' L'^2/k\alpha\nu$
S	dimensionless concentration, $(S'-S'_0)/\Delta S'$
Sh	Sherwood number, equation (12)
S'_0	reference concentration at $x' = 0$, $y' = 0$
$\Delta S'$	characteristic concentration, $j'L'/D$
ΔS	dimensionless wall-to-wall concentration difference
T	dimensionless temperature, $(T'-T'_0)/\Delta T'$
t	dimensionless time, $t'\alpha/L'^2/\sigma$
T'_0	reference temperature, $x' = 0$, $y' = 0$
$\Delta T'$	characteristic temperature, $q'L'/k$
ΔT	dimensionless wall-to-wall temperature difference
u	dimensionless velocity in x-direction, $u'L'/\alpha$
v	dimensionless velocity in y-direction, $v'L'/\alpha$
x	dimensionless coordinate axis, x'/L'
y	dimensionless coordinate axis, y'/L'.

Greek symbols

α	thermal diffusivity $k/(\rho c)_f$
β_S	concentration expansion coefficient
β_T	thermal expansion coefficient
ε'	porosity of the porous medium
ε	normalized porosity of the porous medium, ε'/σ
ν	kinematic viscosity of fluid
μ	dynamic viscosity of fluid
ρ	density of fluid
$(\rho c)_f$	heat capacity of fluid
$(\rho c)_p$	heat capacity of saturated porous medium
σ	heat capacity ratio, $(\rho c)_p/(\rho c)_f$
Ψ	dimensionless stream function, Ψ'/α.

Superscript

$'$	dimensional variable.

Subscripts

max	maximum value
min	minimum value
0	reference state.

Analytical solutions, valid for stratified flow in slender enclosures ($A \gg 1$) were obtained by these authors. Scale analysis was applied to the two extreme cases of heat-driven and solute-driven natural convection. Numerical solutions of the full governing equations were found to be in excellent agreement with the analytical solutions. Trevisan and Bejan [17] and Nield and Bejan [18] recently reviewed the literature on double-diffusive convection in porous media.

In the present study, results from steady-state calculations of porous media subjected to uniform fluxes of heat and mass are presented. The aim of this study is to determine the effect of R_T, Le and N on Nu and Sh for both aiding ($N > 0$) and opposing ($N < 0$) flows. This investigation is limited to the case of a square cavity ($A = 1$). For this situation, the flow patterns are expected to be quite different from the parallel flow structure reported by Alavyoon *et al.* [14–16] for slender enclosures ($A \gg 1$). Also, in the present study, for opposing flows, the existence of multiple steady states is demonstrated. The effect of the governing parameters on the domain of existence of these multiple solutions is discussed.

MATHEMATICAL FORMULATION

Figure 1 displays a schematic of the flow configuration. The rectangular porous enclosure is of width L' and height H', and the Cartesian coordinates (x', y'), with the corresponding velocity components (u', v'), are indicated herein. The top and bottom boundaries of the enclosure are thermally insulated and impermeable. The vertical walls are subjected to uniform fluxes of heat and mass as

$$q' = k\left.\frac{\partial T'}{\partial x'}\right|_{x'=0,L'} \tag{1}$$

$$j' = D\left.\frac{\partial S'}{\partial x'}\right|_{x'=0,L'} \tag{2}$$

where both q' and j' are assumed to be positive.

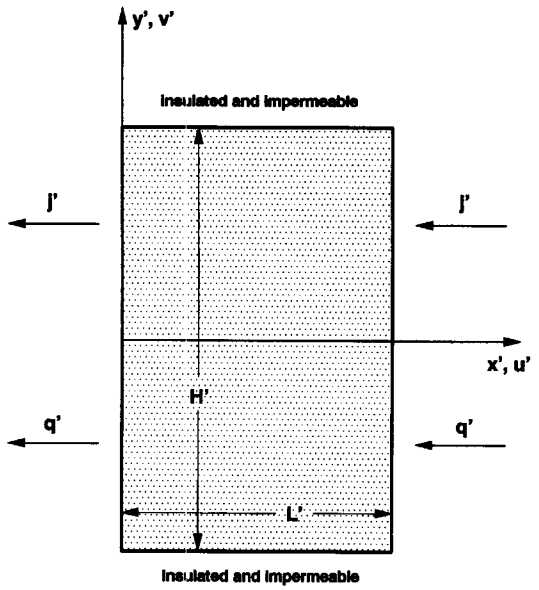

Fig. 1. Flow configuration and coordinate system.

According to Fig. 1, the boundary conditions (1) and (2) mean cooling and mass efflux at $x' = 0$ and heating combined with mass influx at $x' = L'$. The symbols are defined in the nomenclature.

The fluid saturated porous medium is assumed homogeneous and isotropic and inertial effects are neglected. The solution that saturates the porous matrix is modeled as a Boussinesq incompressible fluid whose density variation can be expressed as

$$\rho = \rho_0[1-\beta_T(T'-T'_0)-\beta_S(S'-S'_0)] \tag{3}$$

where β_T and β_S are the thermal and concentration expansion coefficients. Subscript 0 stands for a reference state.

The equations governing the conservation of momentum, energy and constituent in the solution-saturated porous medium are (see for instance Lin [12])

$$\frac{\partial^2\Psi}{\partial x^2}+\frac{\partial^2\Psi}{\partial y^2} = -R_T\left[\frac{\partial T}{\partial x}+N\frac{\partial S}{\partial x}\right] \tag{4}$$

$$\frac{\partial T}{\partial t}+u\frac{\partial T}{\partial x}+v\frac{\partial T}{\partial y} = \frac{\partial^2 T}{\partial x^2}+\frac{\partial^2 T}{\partial y^2} \tag{5}$$

$$\varepsilon\frac{\partial S}{\partial t}+u\frac{\partial S}{\partial x}+v\frac{\partial S}{\partial y} = \frac{1}{Le}\left[\frac{\partial^2 S}{\partial x^2}+\frac{\partial^2 S}{\partial y^2}\right] \tag{6}$$

where the stream function Ψ is defined by

$$u = \frac{\partial\Psi}{\partial y} \quad v = -\frac{\partial\Psi}{\partial x}. \tag{7}$$

The above equations were nondimensionalized by introducing the following definitions:

$$\left.\begin{array}{ll}(x,y) = (x',y')/L' & t = t'\alpha/L'^2/\sigma \\ (u,v) = (u',v')L'/\alpha & \Psi = \Psi'/\alpha \\ S = (S'-S'_0)/\Delta S' & T = (T'-T'_0)/\Delta T'\end{array}\right\} \tag{8}$$

where T'_0 is the temperature at the origin of the coordinate system and $\Delta T' = q'L'/k$ a characteristic temperature difference. S'_0 and $\Delta S' = j'L'/D$ are the corresponding values for the constituent.

The dimensionless boundary conditions for the physical system considered in the present study are

$$\left.\begin{array}{lll}x = 0,1 & \Psi = 0 & \dfrac{\partial T}{\partial x} = \dfrac{\partial S}{\partial x} = 1 \\ y = \pm\dfrac{A}{2} & \Psi = 0 & \dfrac{\partial T}{\partial y} = \dfrac{\partial S}{\partial y} = 0\end{array}\right\}. \tag{9}$$

The non-dimensionalization process results in the appearance of several dimensionless parameters in the governing equations and boundary conditions which are defined as

$$\left.\begin{array}{ll}R_T = \dfrac{g\beta_T K q' L'^2}{k\alpha v} & Le = \alpha/D \quad N = \dfrac{\beta_S\Delta S'}{\beta_T\Delta T'} \\ A = H'/L' & \varepsilon = \varepsilon'/\sigma\end{array}\right\}. \tag{10}$$

The first two dimensionless groups are the thermal Rayleigh number R_T and the Lewis number Le, respectively. The Lewis number represents the ratio between the thermal and solutal diffusivities. The buoyancy ratio N is a measure of the relative significance of species and thermal diffusion in causing the density variation which drives the flow. For the boundary conditions considered here a positive value of N results in augmenting convection (cooperative buoyancy forces), a negative value leads to opposing flows (the net buoyancy is weakened). Further, N is zero for non-species effect and infinite for solute-dominated effect. The group A is the aspect ratio that defines the slenderness of the enclosure. The last group ε is the normalized porosity of the porous medium.

The Nusselt and Sherwood numbers are used to describe the heat and mass transfer characteristics and thus are of interest in engineering applications. In the present study the average Nusselt and Sherwood numbers can be evaluated respectively by

$$Nu = \frac{q'}{k\overline{\Delta T'}/L'} = \frac{A}{\displaystyle\int_{-A/2}^{+A/2}[T(1,y)-T(0,y)]\,dy} \tag{11}$$

and

$$Sh = \frac{j'}{D\overline{\Delta S'}/L'} = \frac{A}{\displaystyle\int_{-A/2}^{+A/2}[S(1,y)-S(0,y)]\,dy} \tag{12}$$

where $\overline{\Delta T'}$ and $\overline{\Delta S'}$ are the side-to-side averaged temperature and concentration differences, respectively.

NUMERICAL METHOD

The conservation equations reported in the previous section were solved numerically using the well-known Alternating Direction Implicit (ADI) scheme of Peaceman and Rachford (Roache [19]). The time-dependent governing equations (5) and (6) are marched in time until a steady solution is obtained. The temporal and spacial derivatives are approximated by first- and second-order discretizations, respectively. The stream function equation, equation (4), on the other hand, is solved by the Gauss–Seidel (S.O.R.) iterative scheme at each time step with a relaxation factor of 1.78. The following criteria were used to check convergence of all variables at all nodal points:

$$\frac{\sum_i \sum_j |\Phi_{i,j}^{\text{new}} - \Phi_{i,j}^{\text{old}}|}{\sum_i \sum_j |\Phi_{i,j}^{\text{new}}|} \leqslant \Gamma \tag{13}$$

where Φ is any variable Ψ, T, S, and Γ is a prespecified constant, usually set to 10^{-4} or less. A third-order forward and backward discretization is carried out to approximate the hydrodynamic, thermal and solutal boundary conditions imposed on the physical domain. Reliable numerical results are obtained by performing an energy balance at each time step over the physical domain. Also, for a steady flow condition the heat transfer through each plane x = constant was evaluated at each location $0 \leqslant x \leqslant 1$ and compared with that of the input ($x = 1$) and the output ($x = 0$). A similar test was conducted to verify the overall mass balance. For most of the results reported here the energy and the mass balances were satisfied to within 0.1%.

For the present work, uniform mesh sizes have been used for both x- and y-directions. Based on several trial cases, a suitable grid field of (80×80) was selected for the present calculations. In the cases where the parameters N and Le were large, the grid fineness was improved up to 140×140. Typical values of the time steps range from 5×10^{-5} to 10^{-3}. The CPU time required to reach steady state was approximately from 3 to 14 CPU h on an IBM RISC 6000/RS 365 workstation.

In the limiting case of non mass transfer effect in the flow, $N = 0$, the flow patterns and temperature fields predicted by the present numerical code, for natural convection in a cavity subjected to a horizontal temperature differential, were in excellent agreement with the solutions given by Shiralkar *et al.* [20]. More details of code validation are given in [21]. The solutions using the current code with double-diffusive natural convection have been directly compared with the numerical solutions of Alavyoon [14] for a square cavity. The agreement with this study was very satisfactory with less than 2% deviations in most cases.

RESULTS AND DISCUSSION

The foregoing analysis indicates that there are four parameters that could be varied in this study. These are R_T, N, Le and A. While computations can be carried out for any combination of the governing parameters, the objective here is to present a sample of results in order to illustrate the effects of these parameters on the cell formation processes and heat and mass transfer characteristics. As mentioned earlier, the study is limited to a cavity with an aspect ratio of unity, i.e. a square enclosure. In the actual computations, ε is set equal to unity, Le is varied from 1 to 10^3 and R_T from 1 to 165. The buoyancy ratio N is in the range -20 to 20, covering the spectrum from mass-driven opposing flows ($N \ll -1$), to pure heat-driven flows ($N = 0$) to mass-driven aiding flows ($N \gg 1$).

Effect of buoyancy flows

In Figs. 2–4 the effects of the buoyancy forces ratio are illustrated for $R_T = 100$ and $Le = 10$. The results are presented in terms of streamlines (on the left), isotherms (at the center) and iso-concentration (on the right) contours for different values of N. The flow directions in the graphs can be easily identified according to the distributions of temperature and solute. The intervals of streamlines, isothermal and iso-concentration lines are $\Delta\Phi = (\Phi_{\max} - \Phi_{\min})/16$, where Φ stands for Ψ, T or S. Due to the thermal and solutal boundary conditions considered here, the right side wall has a higher temperature and higher concentration than the left side wall. As a result, the direction of the thermal flow is counterclockwise, whereas the direction of the solutal flow depends upon the sign of the concentration expansion coefficient β_S in equation (3). Thus the direction of the solutal flow is counterclockwise for β_S (i.e. N) > 0 and clockwise for β_S (i.e. N) < 0.

Figures 2(a)–(c) exemplify typical features of aiding double-diffusive flow ($N > 0$). First, the heat-driven flow limit ($N = 0$) depicted in Fig. 2(a) is discussed. For this situation the ensuing flow is driven solely by the buoyancy effect associated with the temperature gradients. The resulting velocity and temperature fields are the ones reported already for the pure heat transfer problem (see for instance Trevisan and Bejan [9] and Vasseur *et al.* [22]). When the buoyancy ratio is increased above zero the flow near the hot right-hand wall is driven vertically upward, and meanwhile the low concentration at the left-hand wall causes the fluid near it to sink. Clearly, both thermal and solutal buoyancy effects are augmenting each other and thus they simultaneously accelerate the flow counterclockwise. Figure 2(b) shows the results obtained upon increasing N from zero to unity for which the solutal and thermal buoyancies are equal. The resulting pattern of streamlines, isotherms and iso-concentrations are seen to be very similar to those of the heat-driven case shown in Fig. 2(a). Also it is observed from Figs. 2(a) and 2(b) that the thicknesses of the vertical boundary layers of velocity, temperature and concentration are approximately equal despite the relatively high Lewis number ($Le = 10$) considered

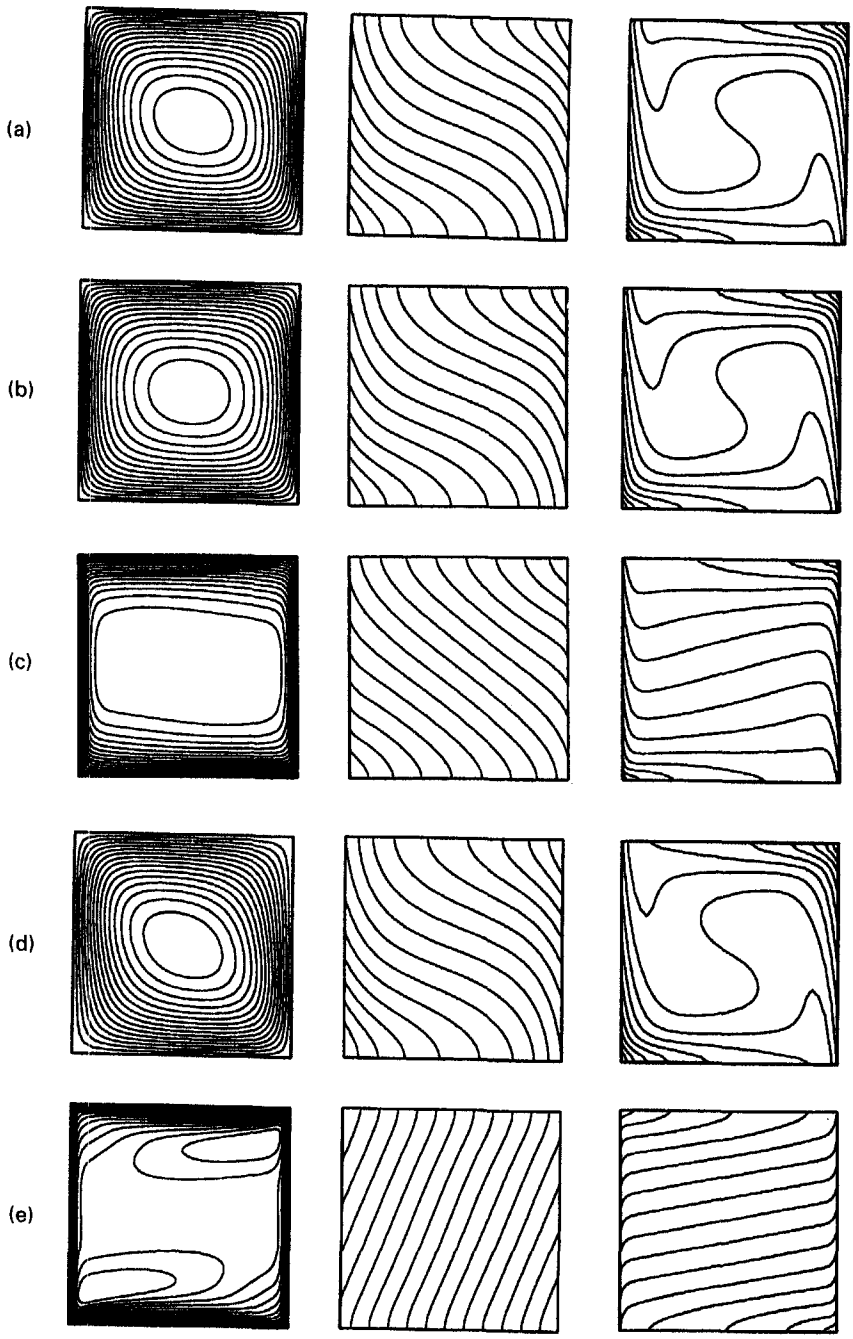

Fig. 2. Stream function, temperature and concentration lines for aiding and opposing flows at $R_T = 100$ and $Le = 10$. (a) $N = 0$, $\Psi_{max} = 2.186$, $\Psi_{min} = 0$, $Nu = 2.301$, $Sh = 11.583$, $\Delta T_{max} = 0.903$, $\Delta S_{max} = 0.267$. (b) $N = 1$, $\Psi_{max} = 2.103$, $\Psi_{min} = 0$, $Nu = 2.327$, $Sh = 13.093$, $\Delta T_{max} = 0.902$, $\Delta S_{max} = 0.239$. (c) $N = 20$, $\Psi_{max} = 1.329$, $\Psi_{min} = 0$, $Nu = 2.089$, $Sh = 29.148$, $\Delta T_{max} = 1.004$, $\Delta S_{max} = 0.174$. (d) $N = -1$, $\Psi_{max} = 2.259$, $\Psi_{min} = 0$, $Nu = 2.231$, $Sh = 9.686$, $\Delta T_{max} = 0.907$, $\Delta S_{max} = 0.312$. (e) $N = -20$, $\Psi_{max} = 0$, $\Psi_{min} = -0.497$, $Nu = 1.153$, $Sh = 13.022$, $\Delta T_{max} = 1.198$, $\Delta S_{max} = 0.363$.

here. Similar results have been reported in the past by Alavyoon [14]. When the buoyancy ratio is increased to $N = 20$ the pattern of streamlines of Fig. 2(c) indicates that a large portion of the fluid in the center of the cavity is now stagnant due to the blocking effect of the vertical stratification of the density field in this area and the flow circulation is restricted to thin boundary layers of almost constant thickness, along the vertical walls. The iso-concentration lines indicate that the concentration field too has boundary layer character, its thickness being approximately equal to that of the hydrodynamic boundary layer. From Figs. 2(a)–(c) it is clear that solutal concentration is gradually enhanced as N increases.

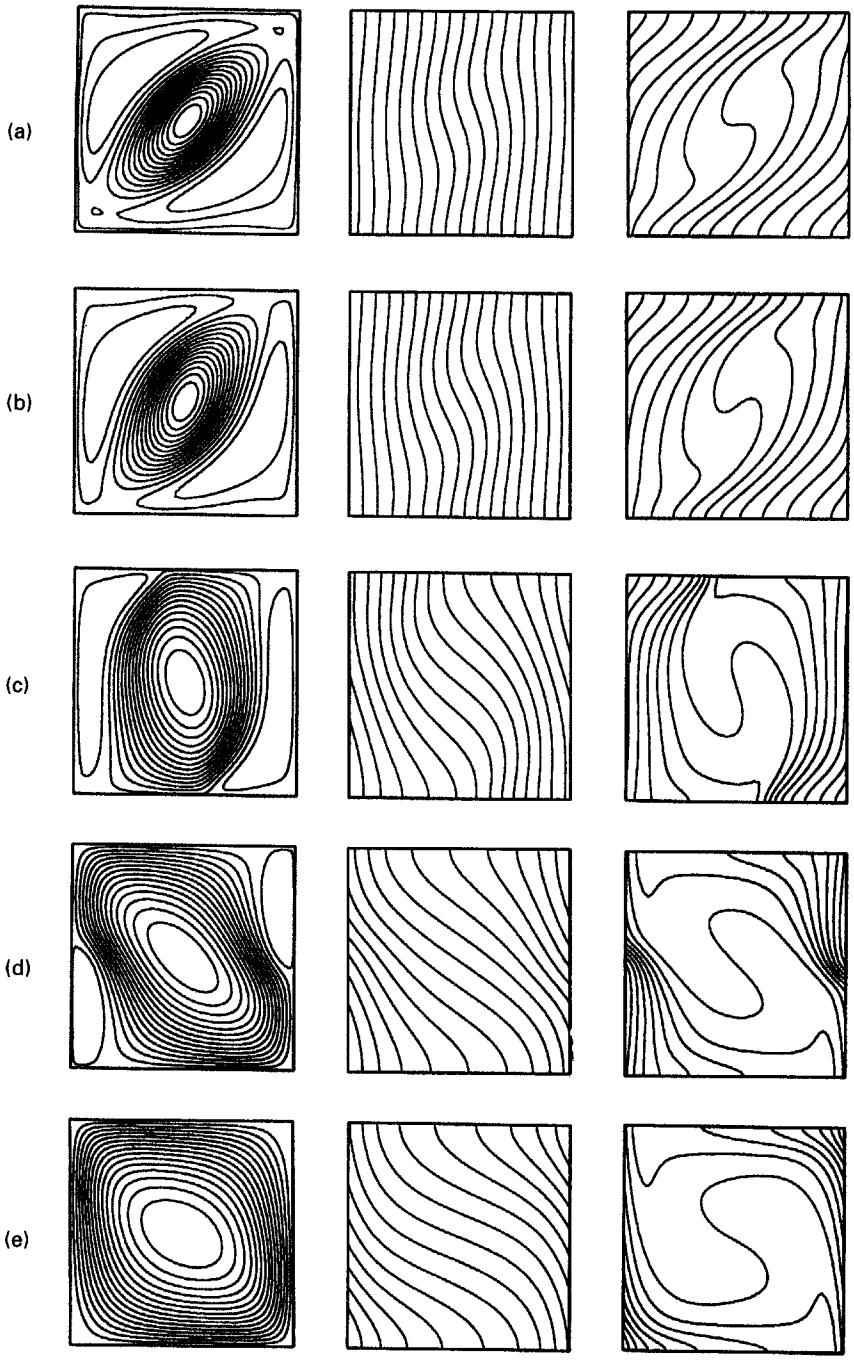

Fig. 3. Stream function, temperature and concentration lines for thermal dominated transitional flow for $R_T = 100$ and $Le = 10$. (a) $N = -2$, $\Psi_{max} = 0.737$, $\Psi_{min} = -0.216$, $Nu = 1.020$, $Sh = 1.839$, $\Delta T_{max} = 1.022$, $\Delta S_{max} = 0.942$. (b) $N = -1.85$, $\Psi_{max} = 1.042$, $\Psi_{min} = -0.221$, $Nu = 1.035$, $Sh = 1.729$, $\Delta T_{max} = 0.992$, $\Delta S_{max} = 0.930$. (c) $N = -1.85$, $\Psi_{max} = 1.931$, $\Psi_{min} = -0.221$, $Nu = 1.252$, $Sh = 2.161$, $\Delta T_{max} = 0.990$, $\Delta S_{max} = 0.664$. (d) $N = -1.85$, $\Psi_{max} = 2.250$, $\Psi_{min} = -0.174$, $Nu = 1.683$, $Sh = 3.952$, $\Delta T_{max} = 0.960$, $\Delta S_{max} = 0.440$. (e) $N = -1.5$, $\Psi_{max} = 2.291$, $\Psi_{min} = -0.002$, $Nu = 2.155$, $Sh = 8.266$, $\Delta T_{max} = 0.915$, $\Delta S_{max} = 0.371$.

The typical feature of opposing double-diffusion flow ($N < 0$) is now discussed. Figure 2(d) shows the results obtained upon decreasing N from zero, Fig. 2(a), to -1. For this particular value of the buoyancy ratio, it has been demonstrated in the past by Trevisan and Bejan [9] that the flow disappears altogether in the limiting case of $Le = 1$. This follows from the fact that, for this situation, the dimensionless temperature and concentration fields are identical such that the source term in the momentum equation is zero inde-

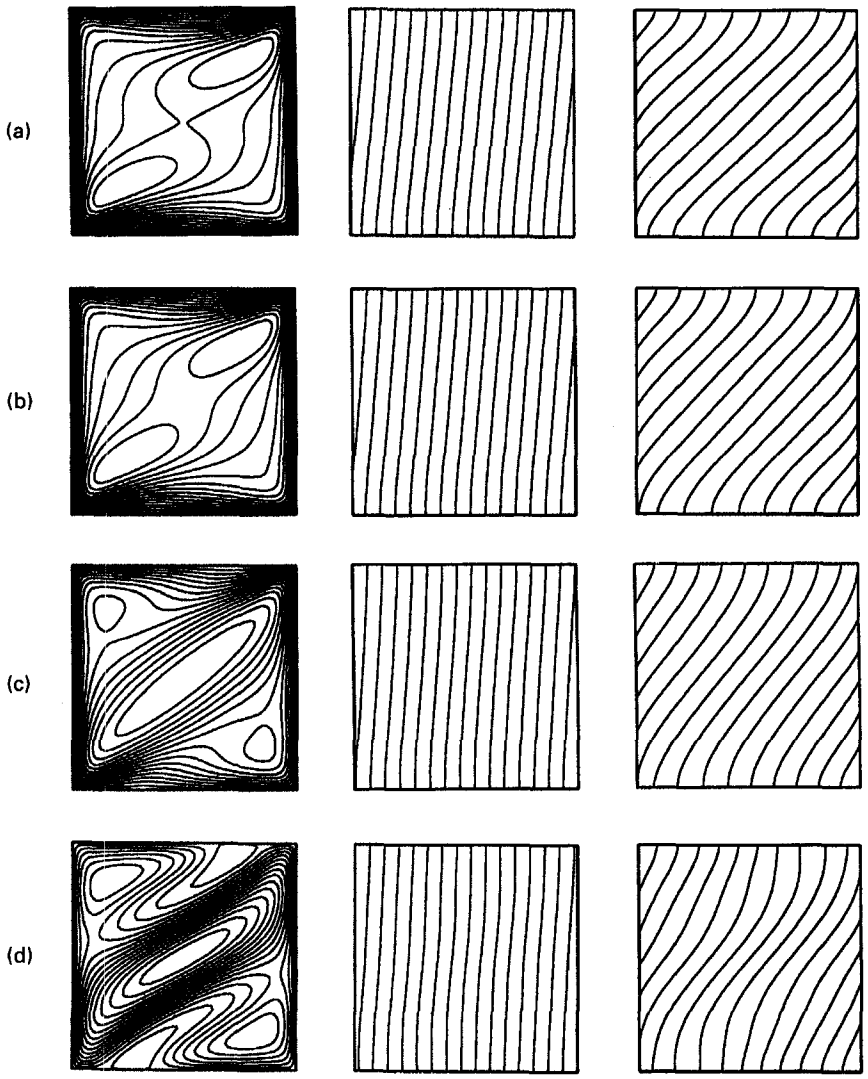

Fig. 4. Stream function, temperature and concentration lines for solutal-dominated transitional flow for $R_T = 100$ and $Le = 10$. (a) $N = -2$, $\Psi_{max} = 0$, $\Psi_{min} = -0.131$, $Nu = 1.009$, $Sh = 1.854$, $\Delta T_{max} = 1.076$, $\Delta S_{max} = 1.051$. (b) $N = -1.85$, $\Psi_{max} = 0$, $\Psi_{min} = -0.123$, $Nu = 1.008$, $Sh = 1.726$, $\Delta T_{max} = 1.070$, $\Delta S_{max} = 1.078$. (c) $N = -1.5$, $\Psi_{max} = 0$, $\Psi_{min} = -0.109$, $Nu = 1.005$, $Sh = 1.432$, $\Delta T_{max} = 1.054$, $\Delta S_{max} = 1.157$. (d) $N = -1.35$, $\Psi_{max} = 0.010$, $\Psi_{min} = -0.132$, $Nu = 1.003$, $Sh = 1.303$, $\Delta T_{max} = 1.043$, $\Delta S_{max} = 1.174$.

pendent of the value of the thermal Rayleigh number R_T. As a result, the steady state solution is a motionless fluid layer where the temperature and concentration profiles are linear. When the Lewis number is different from unity a purely diffusive (motionless) solution is also possible. The existence of such a solution was demonstrated numerically for $R_T = 100$ and $Le = 10$, using $\Psi(x,y,0) = 0$, $T(x,y,0) = S(x,y,0) = x$ as initial conditions. However, upon using the rest state ($\Psi(x,y,0) = T(x,y,0) = S(x,y,0) = 0$) as initial conditions, it was found that a convective state is also possible for this situation. Figure 2(d) shows that the resulting flow, driven by the thermal buoyancy force, proceeds counterclockwise. This is a consequence of the fact that, in the core of the cavity, the temperature gradient is larger than the concentration one. Figure 2(e) provides exemplary results for a large buoyancy ratio ($N = -20$). As expected, the flow is again dominated by the mass species buoyancy force. The direction of the fluid circulation has been completely reversed and the flow pattern consists in a primary cell moving clockwise along the cavity walls and two secondary cells contained within it, one in the top right corner and the other one in the bottom left corner.

Natural convection flows arising when the temperature and solute gradients counteract each other ($N < 0$) are in fact much more complex than the sequence of events illustrated in Figs. 2(a), (d) and (e). In the vicinity of $N = -1$, there is a transitional

region, the extent of which depends upon Le and R_T, in which the thermal buoyancy is almost equal and opposite to the solutal buoyancy. In this region, where the direction of the flow circulation undergoes a reversal from a clockwise solutal dominated cell to a counterclockwise thermal dominated cell, multiple steady solutions are possible as it will be now discussed.

When N is sufficiently large the whole flow is primarily driven by the solutal buoyancy, giving rise to a clockwise flow, as illustrated in Fig. 2(e) for $N = -20$. Upon increasing N to -2 the thermal buoyancy starts to exert some influence resulting in the complicated flow pattern disclosed in Fig. 3(a). In the boundary regions, close to the solid walls, the solutal buoyancy is strong enough to induce a primary cell circulating clockwise along the entire enclosure walls. In the core of the cavity the effects of thermal buoyancy set off giving rise to the existence of a multi layer flow structure. From the values of Ψ_{max} and Ψ_{min} it is observed that the convection strength of this multiple-cell convection is much weaker than that of the single-cell convection. Basically, the flow consists of a thermally driven counterclockwise rotating cell, in the central part of the cavity, and two solutably driven clockwise circulations adjacent to the cavity walls. The thermal and solutal driven cells are counterrotating due to the opposing thermal and solutal buoyancies. As mentioned earlier double-diffusive convection in a vertical porous enclosure subjected to opposing and horizontal gradients of heat and solute has been studied recently by Alavyoon *et al.* [16]. Analytical solutions for the velocity and temperature fields were obtained, in the limit of a thin porous layer ($A \gg 1$), using a parallel flow approximation. Among other things, it was demonstrated by these authors that, in the transitional region, for a given value of N, two different flow patterns are predicted by the analytical model. However, their numerical results could only confirm the existence of a single convective mode. This may be due to inappropriate choice of the initial conditions since it will be now demonstrated that, indeed, multiple solutions are possible in the transitional region.

For a given set of the governing parameters, if multiple steady state solutions exist they have their own basin of attraction and only initial conditions within this basin will evolve to the desired steady state. Thus, initial conditions have to be chosen carefully to obtain the multiple solutions. For instance, Figs. 3(b)–(d) and 4(b) illustrate four different possible solutions for $N = -1.85$. The first solution, Fig. 3(b), obtained by using the flow configuration of Fig. 3(a) as initial conditions, is observed to be almost similar to that in Fig. 3(a). For the second solution, a flow pattern akin to that of Fig. 3(c), obtained previously for the case $N = -1.8$ (not presented here), was used as initial conditions. The results indicate that the thermal buoyancy exerts more important effects in Fig. 3(c) than in Fig. 3(b). Consequently, the thermally driven counterclockwise rotating cell in Fig. 3(c) grows in size and strength. Meanwhile, the cells induced by solutal buoyancy dwindle, since they do not own enough momentum to protrude and reach to the opposite walls, and are confined in the vicinity of the vertical walls. For the third solution, Fig. 3(d), the rest state $\Psi(x, y, 0) = T(x, y, 0) = S(x, y, 0) = 0$ was used as initial conditions. For this situation, the thermally driven unicell core flow spans now completely the enclosure while the solutally driven secondary cells are confined in the corners of the cavity. The resulting heat and mass transfer is enhanced since the main cell is large enough to be directly in contact with the thermally and solutally active walls. It must be mentioned that the computing time necessary to obtain the steady flow pattern of Fig. 3(d) is extremely long ($\tau \simeq 45$) due to very slowly decaying oscillations generated for this situation. Upon increasing N to -1.5, Fig. 3(e), the concentration-governed cells have vanished. More exactly, two small solutal cells are still present in the upper right and lower left corners of the cavity but their magnitude is so small that their presence is not observable in the streamline patterns of Fig 3(e). At this stage, a complete reversal of the direction of the flow is achieved, indicating an overturn of relative dominance between the temperature and solute fields on the convection pattern. For completeness it must be mentioned that grid size has also an influence on the solution. For instance, upon doing the computations of Fig. 3(d) (starting from the rest state) it is possible to obtain two solutions: one with a 25×25 grid, for which the results is found to be qualitatively similar to that in Fig. 3(c), and the other with a 85×85 grid which yields the same results as in Fig. 3(d). However, as discussed earlier, to obtain accurate results, all the numerical results presented here were obtained using at least a 80×80 grid size.

As illustrated in Figs. 2 and 3, the effects of the buoyancy ratio N are found to be rather significant on the flow pattern. Distinct flow regimes have been illustrated upon varying the buoyancy ratio over a wide range. These include mass-dominated aiding flow, Fig. 2(c); mass-dominated opposing flow, Fig. 2(e); thermal-dominated flow, Fig. 2(a) and transitional flow, Figs. 3(a)–(e). In transitional flows mass species and thermal buoyancy forces prove to dominate separate circulations within the enclosure. The onset of transition is the buoyancy ratio at which a multi-cell flow structure is generated by the thermal buoyant forces. For the governing parameters considered in Fig. 2, the onset of transition occurs at $N = -2$ since the numerical results for $N = -2.05$ (not presented here) indicate the existence of a unicellular motion rotating in the clockwise direction driven by solutal buoyancy. The end of the transition ($N \simeq -1.5$) occurs when the buoyancy ratio is large enough to overcome the solutal forces and gives rise to a unicell motion driven by thermal buoyancy, Fig. 3(e).

From the results presented in Fig. 3 it is clear that the reversal of the flow, from a clockwise solutal-

dominated circulation to a counterclockwise thermal-dominated circulation is characterized by a multi-cell double-diffusive pattern. At the onset of transition, $N = -2$ in Fig. 3(a), both temperature and solute effects exert some influence, giving rise to separate circulations in opposite directions. This multiple-cell pattern is maintained up to a point, $N \simeq -1.5$ in Fig. 3(e), where the solutally driven cells disappears and the whole flow is primarily driven by the thermal buoyancy. It will be now demonstrated that the solution in the transition region described above is not unique. As discussed above the transitional region starts approximately at $N = -2$, for which the intrusion of a thermal-dominated vortex yields the multi-cellular flow regime depicted in Fig. 3(a). The same case was run again but using this time, as initial conditions, the steady state results for a strong unicellular clockwise motion resulting from the solution of a lower N case, namely $N = -10$. The resulting stable steady state is depicted in Fig. 4(a) which shows the existence of a single clockwise flow, clearly dominated by the mass species buoyancy force. This flow configuration is maintained when N is increased to -1.85, Fig. 4(b), yielding a fourth possible flow pattern (see also Figs. 3(b)–(d)) for this particular value of the buoyancy ratio. It must be mentioned that the convective flow of Fig. 4(b) was obtained by using the steady state results of $N = -2$, Fig. 4(a), as initial conditions. Following this procedure, as the value of N is increased to -1.5, Fig. 4(c) indicates the existence of a major clockwise vortex extending from the right top corner to the left bottom corner. In the remaining two corners the presence of small eddies is noted. Upon increasing N to -1.35, a complicated multicellular flow structure, Fig. 4(d), is produced. Two counterclockwise rotating thermal-driven cells, squeezed by three clockwise rotating solutal-driven cells, are observed to occur at the top and the bottom of the enclosure respectively. This counterrotating flow, induced by the opposing buoyancy forces, is prone to instability. Thus, the numerical results (not presented here) show that upon increasing slightly N from -1.35 to -1.34 the flow pattern of Fig. 4(d) collapses, giving rise to a single counterclockwise rotating thermally-induced circulation similar to that of Fig. 2(b). This sudden transition, from a clockwise solutal-dominated vortex to a counterclockwise thermal-dominated circulation, is quite different from the multi cellular flow transition shown in Fig. 3.

Heat and mass transfer

The effect of buoyancy ratio N on the average Nusselt and Sherwood numbers is depicted in Fig. 5 for $R_T = 100$, $Le = 10$ and $-20 \leqslant N \leqslant 20$. For convenience, the scale for $-3 \leqslant N \leqslant -1$ has been enlarged in Fig. 5(a). The results for opposing flows ($N < 0$) indicate that at $N = -20$ the average Sherwood number is relatively high. For this situation the existence of a sharp solute boundary layer is observable from Fig. 2(e). On the other hand the average

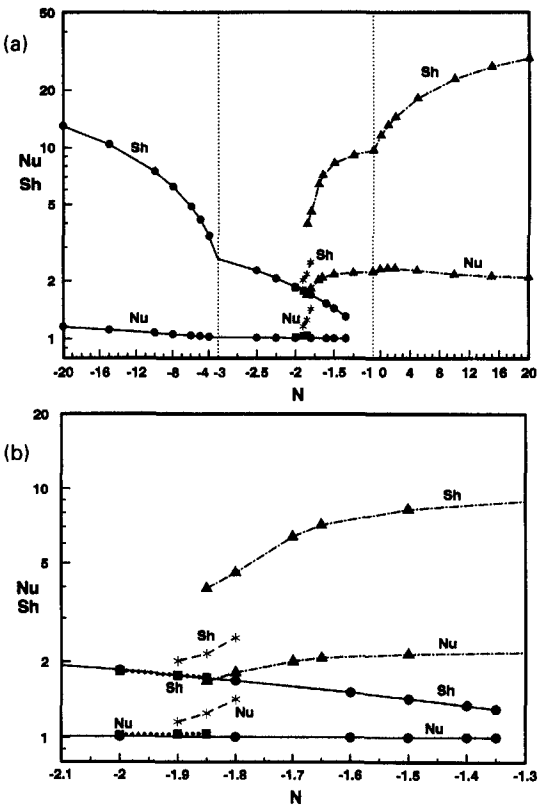

Fig. 5. Nusselt and Sherwood numbers vs the buoyancy ratio N for $R_T = 100$ and $Le = 10$.

Nusselt number is seen to be of order unity. This is due to the large Lewis number considered here ($Le = 10$), for which the side-to-side heat transfer process is almost ruled by pure diffusion solely. Upon increasing N, it is observed from Fig. 5(a) that the solutal-dominated opposing flow can be maintained up to $N \simeq -1.35$. For this regime one can note that Nu remains approximately close to unity while Sh decreases sharply with the magnitude of $|N|$. This is due to the fact that, upon increasing N, the flow driven by the buoyancy effect due to solutal variations is more and more weakened by the opposing thermal buoyancy force. For the solutal-dominated aiding flow ($N > 0$), Fig. 5(a) indicates that Sh increases significantly when N is raised from 0 to 20, i.e. as the magnitude of the solutal buoyancy forces is increased. On the other hand, as for the case of opposing flows, the average Nusselt number is observed to remain approximately constant, especially when N is made very large. Also, a bird's-eye-view of the numerical results in Fig. 5(a) indicates that both Sh and Nu are less in the opposing flow area ($N < 0$) than for the corresponding N in the aiding flow range ($N > 0$).

The effects of the occurrence of multiple solutions, for the range $-2 \leqslant N \leqslant -1.35$, on Nu and Sh will be now discussed. To this end a zoom of the region in the vicinity of $N = -1.85$ is presented in Fig. 5(b). It is seen that, depending on the value of N, the number

of possible solutions varies from 2 to 4. Thus, in addition to the solutal-dominated opposing flow ($N \leqslant -1.35$) described above a thermal-dominated flow, exemplified by the flow pattern of Fig. 3(d), occurs for $N \geqslant -1.85$. As discussed earlier, for a buoyancy ratio $N \geqslant -2$ a third possible solution, similar to that illustrated in Fig. 3(a), can be maintained up to $N \simeq -1.85$. For this situation, it is found that *Nu* and *Sh* are approximately equal to the results obtained for the solutal-dominated opposing flow solution. Finally, a fourth solution, akin to that depicted in Fig. 3(c), is predicted for $-1.9 \leqslant N \leqslant -1.8$.

The effects of Lewis number *Le* and Rayleigh number R_T on the average Nusselt and Sherwood numbers for opposing flows in the transitional region are illustrated in Figs. 6(a) and (b), respectively for $N = -1.8$. The data in Fig. 6(a), obtained for $R_T = 10$, span the Lewis number range 1–10^3. The plot shows that at Lewis numbers smaller than approximately 11.6, only one steady state solution exists. For these low Lewis numbers the flow field, consisting of a counterclockwise circulation, is controlled essentially by the concentration field. A reversal of the convection direction of the primary cell is observed when *Le* is increased above approximately 145. For these large Lewis numbers the velocity field is now primarily controlled by the thermal buoyancy. For $11.6 \leqslant Le \leqslant 145$, Fig. 6(a) indicates the existence of two different possible solutions. Depending upon the initial conditions it was found numerically that both solutal dominated and thermal dominated flows are possible. Figures 7(a) and (b) show the flow, temperature and concentration structures at $Le = 100$. The concentration-dominated flow of Fig. 7(a) is qualitatively akin to the results discussed previously for $R_T = 100$, Fig. 4(b). However, due to the low Rayleigh number considered here ($R_T = 10$) the multicellular structure, reported in Fig. 3(b) for thermal dominated flows, is not observed here. The solute field of Fig. 7(b) is seen to be highly uniform in the core of the cavity, giving rise to a single cell largely controlled by the temperature field. In Fig. 6(b) the results obtained for $Le = 10$ exemplify the influence of the Rayleigh number on the possible existence of multiple solutions in the transitional regime. When R_T is small enough the velocity field is controlled by concentration and the resulting flow patterns, similar to that of Fig. 2(a), are unique. Upon increasing R_T, it was found that this flow regime could be maintained up to approximately 165 for which the layered flow structure depicted in Fig. 7(c) is obtained. The solutally driven flow is very strong around the periphery of the vertical side walls. Furthermore, unlike the previous case, a three-layer structure is visible in the interior core. These three layer-structured clockwise circulations, are driven by the solutal buoyancy, the thermal field in the core of the cavity being nearly conductive. For R_T higher than 165 it is found that the solution evolves towards an oscillating state of convection (the Hopf's bifurcation). This situation has been recently studied, among others, by Alavyoon *et al.* [16] and will not be discussed here. As expected, Fig. 6(b) reveals that, in the range $12 \leqslant R_T \leqslant 100$, a thermally induced counterclockwise flow pattern similar to that of Fig. 3(d) is also possible. Furthermore, for $55 \leqslant R_T \leqslant 140$ a multi cellular flow, exemplified by Fig. 3(c), can be maintained only for the range of the Rayleigh number mentioned above. For $R_T < 55$ the numerical solutions were found to evolve to the solutally-dominated clockwise circulation. For $R_T > 140$ the flow was found to become oscillating.

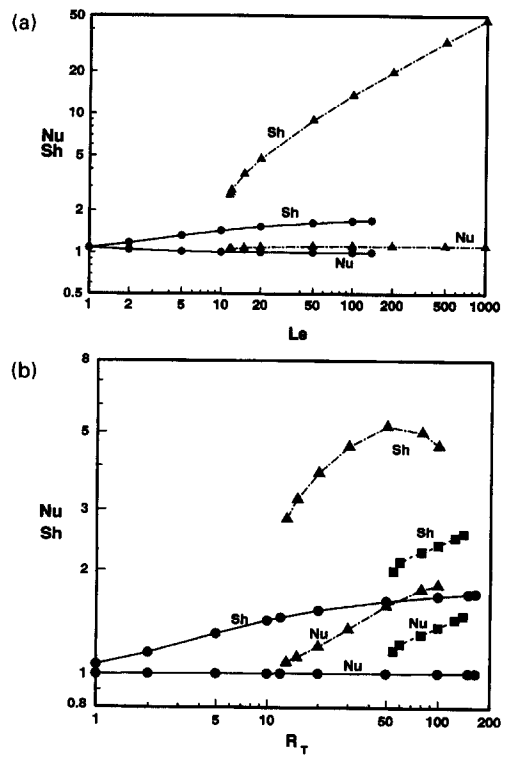

Fig. 6. Nusselt and Sherwood numbers for $N = -1.8$ vs (a) Lewis number ($R_T = 10$) and (b) Rayleigh number ($Le = 10$).

SUMMARY

A numerical study is conducted to investigate the patterns and characteristics associated with the double-diffusive convection is a square porous enclosure with uniform heat and mass fluxes along the vertical sides. Important controlling parameters including the thermal Rayleigh number, Lewis number and buoyancy ratio are varied and new insights into the solutions of both augmenting and counteracting cases gained. The major results obtained in the present investigation can be summarized as follows.

(1) The existence of multiple patterns of convection in the transition regime, where both thermal and concentration buoyancy forces are approximately equal and opposite, has been demonstrated numerically.

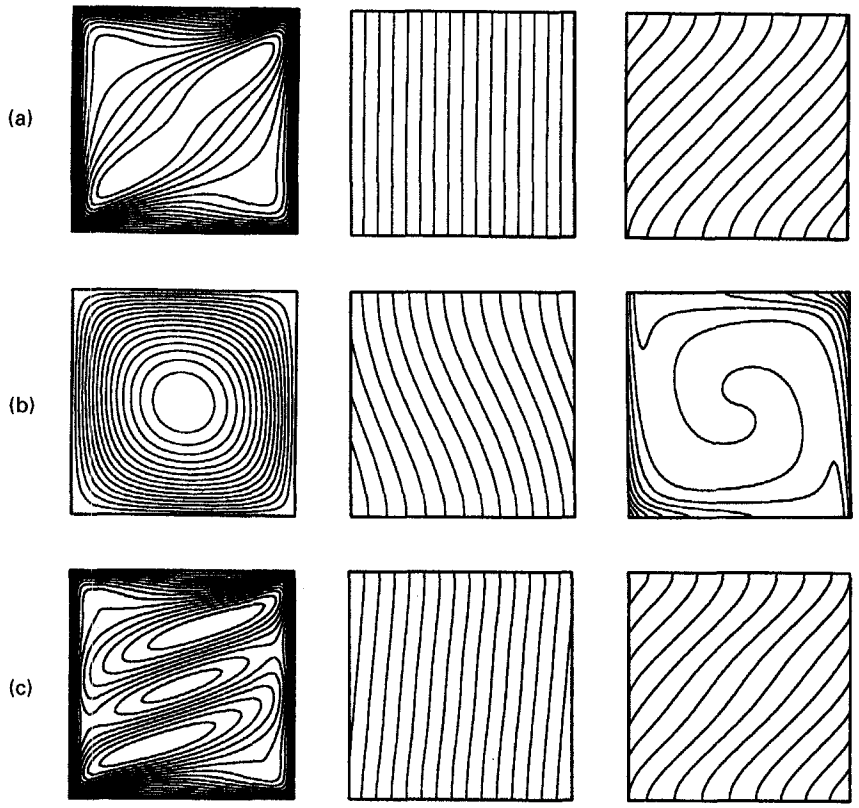

Fig. 7. Stream function, temperature and concentration lines for $N = -1.8$. (a) $R_T = 10$, $Le = 100$, $\Psi_{max} = 0$, $\Psi_{min} = -0.012$, $Nu = 1.000$, $Sh = 1.667$, $\Delta T_{max} = 1.007$, $\Delta S_{max} = 1.097$. (b) $R_T = 10$, $Le = 100$, $\Psi_{max} = 0.639$, $\Psi_{min} = 0$, $Nu = 1.110$, $Sh = 13.503$, $\Delta T_{max} = 1.146$, $\Delta S_{max} = 0.233$. (c) $R_T = 165$, $Le = 10$, $\Psi_{max} = 0$, $\Psi_{min} = -0.130$, $Nu = 1.007$, $Sh = 1.717$, $\Delta T_{max} = 1.070$, $\Delta S_{max} = 1.082$.

Upon increasing N, the reversal of the flow direction from the clockwise solutally-dominated circulation to the counterclockwise solutally-dominated circulation, depends strongly on the initial conditions. Two different modes of transition have been made conspicious. In the first mode, an overturn of relative dominance between the temperature and solute fields on the convection pattern is reached for a given value of N at which an abrupt reversal of the convection direction occurs. In the second mode, upon increasing N, the temperature effects become progressively comparable and eventually larger than the solute effects. For this situation up to four different convective patterns have been observed for a given value of the buoyancy ratio. Complete flow reversal occurs at a given value of N for which the thermal-dominated counterclockwise vortex spans completely the enclosure.

(2) In the transitional regime, for a given value of N, the effects of both Le and R_T on the flow patterns have been investigated. It is demonstrated that, when R_T is maintained constant, the flow is solutally-driven when Le is small and thermally-driven when Le is sufficiently high. For intermediate values of Le, both solutions are possible. On the other hand, for a given values of Le, the flow is solutally-driven for small values of R_T. For intermediate values of R_T the existence of different possible solutions is demonstrated. For larger values of R_T significant fluctuations in the velocity, temperature and concentration are observed.

(3) When $|N|$ is sufficiently small the flow properties are governed primarily by the thermal buoyancy. When $|N|$ is large enough the gross flow characteristics are similar to those of pure solutal convection. The thermal field is qualitatively akin to the pseudo-conduction regime and the overall velocity field in the bulk of the cavity is fairly quiescent.

Acknowledgements—This work was supported in part by the National Sciences and Engineering Research Council of Canada and jointly by the FCAR Government of Quebec.

REFERENCES

1. D. A. Nield, Onset of thermohaline convection in a porous medium, *Water Resour. Res.* **4**, 553–560 (1968).
2. J. W. Taunton, E. B. Lightfoot and T. Green, Thermohaline instability and salt fingers in a porous medium, *Phys. Fluids* **15**, 748–753 (1972).
3. H. Y. Rubin, Effect of solute dispersion on thermal convection in a porous medium layer, *Water Resour. Res.* **9**, 968–974 (1973).
4. D. Poulikakos, Double-diffusive convection in a horizontally sparsely packed porous layer, *Int. Commun. Heat Mass Transfer* **13**, 587–598 (1986).

5. M. S. Malashetty, Anisotropic thermoconvective effects on the onset of double-diffusive convection in a porous medium, *Int. J. Heat Mass Transfer* **36,** 2397–2401 (1993).
6. O. V. Trevisan and A. Bejan, Mass and heat transfer by high Rayleigh number convection in a porous medium heated from below, *Int. J. Heat Mass Transfer* **30,** 2341–2356 (1987).
7. N. D. Rosenberg and F. J. Spera, Thermohaline convection in a porous medium heated from below, *Int. J. Heat Mass Transfer* **35,** 1261–1273 (1992).
8. F. Chen and C. F. Chen, Double-diffusive fingering convection in a porous medium, *Int. J. Heat Mass Transfer* **36,** 793–807 (1993).
9. O. V. Trevisan and A. Bejan, Natural convection with combined heat and mass transfer buoyancy effects in a porous medium, *Int. J. Heat Mass Transfer* **28,** 1597–1611 (1985).
10. Z. Zhang and A. Bejan, The horizontal spreading of thermal and chemical deposits in a porous medium, *Int. J. Heat Mass Transfer* **30,** 2289–2303 (1987).
11. O. V. Trevisan and A. Bejan, Mass and heat transfer by natural convection in a vertical slot filled with porous medium, *Int. J. Heat Mass Transfer* **29,** 403–415 (1986).
12. K. W. Lin, Unsteady natural convection heat and mass transfer in a saturated porous enclosure, *Wärme- und Stoffübertragung* **28,** 49–56 (1993).
13. K. N. Mehta and K. Nandakumar, Natural convection with combined heat and mass transfer with buoyancy effects in non-homogeneous porous medium, *Int. J. Heat Mass Transfer* **30,** 2651–2656 (1987).
14. F. Alavyoon, On natural convection in vertical porous enclosures due to prescribed fluxes of heat and mass at the vertical boundaries, *Int. J. Heat Mass Transfer* **30,** 2479–2498 (1993).
15. F. Alavyoon and Y. Masuda, Free convection in vertical porous enclosures due to opposing fluxes of heat and solute at the vertical boundaries, *Proceedings of the 6th International Symposium on Transport Phenomena in Thermal Engineering*, Seoul, Korea, Vol. 1, pp. 151–156 (1993).
16. F. Alavyoon, Y. Masuda and S. Kimura, On natural convection in vertical porous enclosures due to opposing fluxes of heat and mass prescribed at the vertical walls, *Int. J. Heat Mass Transfer* **37,** 195–206 (1994).
17. O. V. Trevisan and A. Bejan, Combined heat and mass transfer by natural convection in a porous medium, *Adv. Heat Transfer* **20,** 315–352 (1990).
18. D. A. Nield and A. Bejan, *Convection in Porous Media*. Springer, Berlin (1992).
19. P. J. Roache, *Computational Fluid Dynamics*. Hermosa, Albuquerque (1982).
20. G. S. Shiralkar, M. Haajizadeh and C. L. Tien, Numerical study of high Rayleigh number in a vertical porous enclosure, *Numer. Heat Transfer* **6,** 223–234 (1983).
21. P. Vasseur, M. G. Satish and L. Robillard, Natural convection in a thin, inclined porous layer exposed to a constant heat flux, *Int. J. Heat Mass Transfer* **30,** 537–549 (1987b).
22. P. Vasseur, L. Robillard and I. Anochiravani, Natural convection in an inclined rectangular porous cavity with uniform heat flux from the side, *Wärme- und Stoffübertragung* **22,** 69–77 (1988).